Ultrasound Image Restoration Using Weighted Nuclear Norm Minimization

Hanmei Yang[1], Heng Zhang[1], Ye Luo[1] , Jianwei Lu[1], Jian Lu[2]

[1] 1 School of Software Engineering, Tongji University

[2] College of Mathematics and Statistics, Shenzhen University

INTRODUCTION

Ultrasound images have been widely used in clinical examination and diagnosis, owing to its advantages of low cost, real time, safety. The system imaging mechanism is based on the echo information of ultrasonic waves to obtain the real-time state of body tissues. However, multiplicative speckle noise often occurs in ultrasound images because of wave interference, which reduces the image quality and bring difficulties to the diagnose and subsequent applications. In order to preserve more details and texture, we investigates a nonconvex low-rank medical ultrasound image despeckling model based on the weighted nuclear norm minimization (WNNM) and data fidelity term. This optimization problem can effectively solved by alternating direction method of multipliers (ADMM). The experimental results on simulated images and real medical ultrasound images demonstrate the excellent performance of the proposed method compared with other four state-of-the-art methods.

THE PROPOSED METHOD

- Based on nonlocal self-similarity and low-rank and statistics priors of ultrasound image, we propose a WNNM-based despeckling model. The **pipeline** is illustrated in Fig. 1.
- Concretely, the ultrasound image is divided into nonlocal similar patch matrixes, which are denoised respectively. The restored ultrasound image can be reconstructed by aggregating all restored pathes.
- **The proposed model** can be formulated as:

  $\min_X \left\langle {(X-Y)^2}/{X}, 1 \right\rangle + \lambda \|X\|_{\omega,*},$

  s.t. $\mathrm{rank}(X) \le r.$

  where X denotes the original image patch, and Y represents the observed image patch.
- The optimization problem is solved by ADMM. The augmented Lagrangian function is formulated as:

$$\mathcal{L}(X,L,Z) = \left\langle {(X-Y)^2}/{X}, 1 \right\rangle + \lambda \|L\|_{\omega,*} + \langle Z, X-L \rangle + {\mu}/{2} \|X-L\|_F^2.$$

It is addressed by alternatively optimizing one variable while fixing others.

1) Update subproblem X via optimizing:

$$X^{t+1} = arg \min_X \left\langle {(X^t-F)^2}/{X^t}, 1 \right\rangle + {\mu^t}/{2} \left\| {Z^t}/{\mu^t} + X^t - L^t \right\|_F^2.$$

2) Update subproblem L via optimizing:

$$L^{t+1} = arg \min_{rank(L) \le r} \lambda \|L^t\|_{\omega,*} + {\mu^t}/{2} \left\| {Z^t}/{\mu^t} + X^{t+1} - L^t \right\|_F^2.$$

3) Update Lagrange multiplier Z via:

$$Z^{t+1} = Z^t + \mu^t (X^{t+1} - L^{t+1}).$$

4) Update parameter μ via:

$$\mu^{t+1} = \rho \mu^t.$$

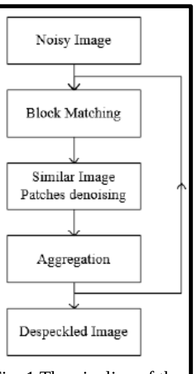

Fig. 1 The pipeline of the proposed method

EXPERIMENTAL RESULTS

Experimental environment:

Compared methods: JY, SRAD, NLLRF, DFoE, NNM-US.

Evaluation criteria: SNR, PSNR,SSIM.

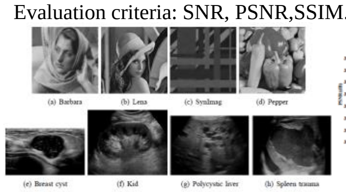

Fig. 2. The simulated and real medical ultrasound images used in experiment.

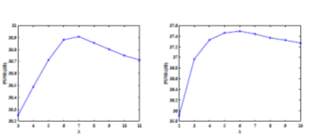

Fig. 3. Sensitivity analysis of parameter λ.

Simulated images despeckling experiment

As reported in TABLE I, It is obviously that our method achieves highest values in most cases. As shown in Fig. 4 and Fig.5, the new approach can effectively remove the noise while preserving more features of degraded images compared with other five state-of-the art methods.

TABLE I
THE VALUES OF METRICS OF DIFFERENT DESPECKLING APPROACHES

Image	Method	$\sigma=2$ SNR	$\sigma=2$ PSNR	$\sigma=2$ SSIM	$\sigma=3$ SNR	$\sigma=3$ PSNR	$\sigma=3$ SSIM
Barbara	JY	11.862	26.279	0.755	9.608	24.304	0.669
	SRAD	12.185	26.479	0.740	10.319	24.676	0.661
	DFoE	15.327	29.524	0.867	12.875	27.148	0.798
	NLLRF	16.305	30.466	0.888	13.576	27.915	0.817
	NNM-US	16.163	30.196	0.868	14.047	28.197	0.822
	Ours	**16.745**	**30.907**	**0.899**	**14.511**	**28.766**	**0.851**
Lena	JY	15.077	29.155	0.848	12.603	27.003	0.789
	SRAD	15.266	29.249	0.828	13.419	27.549	0.800
	DFoE	**17.264**	**31.093**	**0.887**	14.982	28.964	**0.847**
	NLLRF	16.428	30.300	0.859	14.432	28.481	0.823
	NNM-US	16.288	30.181	0.841	14.473	28.481	0.809
	Ours	17.047	30.922	0.874	**15.113**	**29.144**	0.843
SynImag	JY	14.894	36.295	0.957	11.553	33.439	0.940
	SRAD	14.131	35.500	0.947	11.388	32.620	0.868
	DFoE	16.353	37.352	**0.965**	14.312	34.932	0.951
	NLLRF	15.341	36.348	0.940	**14.805**	**36.035**	**0.955**
	NNM-US	15.477	35.831	0.946	13.467	34.112	0.925
	Ours	**16.414**	**37.493**	0.963	14.550	35.742	0.949
Pepper	JY	15.504	29.476	0.851	12.606	26.888	0.804
	SRAD	15.351	29.251	0.827	13.634	27.616	0.805
	DFoE	17.106	30.827	0.876	14.976	28.767	0.843
	NLLRF	16.970	30.711	0.873	14.833	28.672	0.832
	NNM-US	16.347	30.041	0.833	14.510	28.292	0.804
	Ours	**17.138**	**30.904**	**0.878**	**15.199**	**29.032**	**0.845**

Fig. 4. The despeckled images of Barbara with $\sigma = 3$.

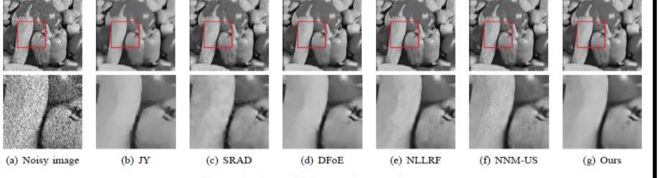

Fig. 5. The despeckled images of Pepper with $\sigma = 3$.

Ultrasound images despeckling experiment

Figs. 6-9 show the denoising results of real ultrasound images. It is seen that the residual images of our proposed method contain little textures, which demonstrates it has better despeckling capability. The recovered images demonstates the proposed method maintains more features in real ultrasound images to provide a better visual effect.

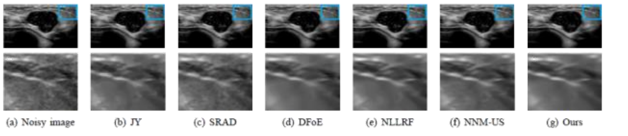

Fig. 6. The real ultrasound despeckled results of Breast cyst. The first row represents restored images. The partial enlarged regions exist in the second row

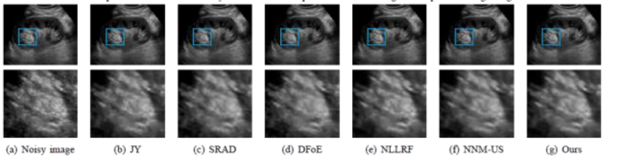

Fig. 7. The real ultrasound despeckled results of Kid. The first row represents restored images. The partial enlarged regions exist in the second row.

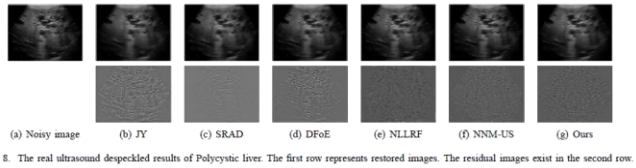

Fig. 8. The real ultrasound despeckled results of Polycystic liver. The first row represents restored images. The residual images exist in the second row.

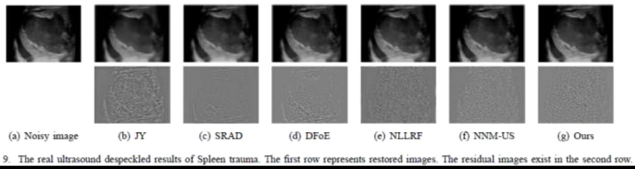

Fig. 9. The real ultrasound despeckled results of Spleen trauma. The first row represents restored images. The residual images exist in the second row.